Journal of Atmospheric and Solar–Terrestrial Physics 274 (2025) 106568

Contents lists available at ScienceDirect

Journal of Atmospheric and Solar-Terrestrial Physics

journal homepage: www.elsevier.com/locate/jastp

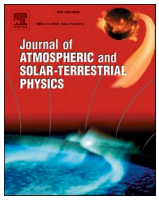

Research Paper

The dynamical influence of energy fluxes in modulating variability of the Indian summer monsoon

R. Bhatla [a,b,*], Archana Maurya [a], Aashna Verma [a], R.K. Mall [b], Sanjay Bist [c]

[a] Department of Geophysics, Institute of Science, Banaras Hindu University, Varanasi, India
[b] DST-Mahamana Centre of Excellence in Climate Change Research, Institute of Environment and Sustainable Development, Banaras Hindu University, Varanasi, India
[c] India Meteorological Department, New Delhi, India

ARTICLE INFO

Handling Editor: Dora Pancheva

Keywords:
Surface heat flux
Land-ocean thermal contrast
Convective activities

ABSTRACT

The surface heat fluxes have a significant role in shaping the Indian summer monsoon (ISM) dynamics. The present study investigates the climatological tricadal and decadal variability of surface energy fluxes viz., net shortwave radiation flux, latent heat flux (LHF) and net heat flux (NHF) during ISM season. For that purpose, a long-term (1961–2020) reanalysis data sets derived from the European Centre for Medium-Range Weather Forecasts fifth-generation (ERA5) and National Center for Environmental Prediction-National Centre for Atmospheric Research reanalysis (NCEP-NCAR) has been considered. Significant regional differences and changing patterns have been observed in the distribution of energy fluxes over southern peninsular India, Arabian Sea (AS), Bay of Bengal (BoB), Equatorial Indian Ocean (EIO), and Southern Indian Ocean. The BoB and AS emerge as vital moisture sources, directly contributing to the monsoon rainfall over eastern, central and western India, respectively. A significant positive change in LHF is observed over AS (9W/m^2) and EIO (12W/m^2) regions, whereas over the BoB region, a negative departure of −8 W/m^2 has been persistent in the recent tricade. These changes correspond to the significant negative anomalous patterns of NHF, i.e., −11 W/m^2 over AS and −18 W/m^2 over EIO, alongside the highest increase in NHF value over the BoB regions (20 W/m^2). The pronounced tricadal phase shift of surface fluxes over AS, EIO, and BoB is identified as a contributing factor influencing ISM rainfall.

1. Introduction

The Indian summer monsoon rainfall (ISMR) is regulated by exchanging heat, moisture and momentum between the land and ocean, resulting in intra-seasonal, interannual, and epochal variability (Gadgil, 2003; Joseph, 2014; Goswami et al., 2016). During the ISMR, intense precipitation leads to substantial latent heat release over the Indian landmass, which significantly warms the troposphere above the continent. This heating intensifies the land-sea thermal gradient, a fundamental driver of the Indian monsoon circulation (Gadgil, 2003; Wang et al., 2008). Latent heat release during deep convection significantly heats the mid-to-upper troposphere over land, reinforcing surface pressure gradients via hydrostatic adjustment and contributing to the overall land-sea thermal contrast. While surface temperature differences initiate monsoon flow (Gadgil, 2003; Wang and Wu, 2008), the vertical structure of heating plays a crucial role in its amplification (Boos and Kuang, 2010). Although the weak temperature gradient (WTG) approximation can hold over oceanic regions (Sobel et al., 2001), it becomes less applicable over land-dominated monsoon systems due to persistent localized heating and convergence. The resulting differential heating, along with moisture contrasts, sustains large-scale ascent over land and descent over adjacent oceans. The surface fluxes allow land-ocean atmospheric interactions to impact the monsoon system (Chang, 2011; Bhatla et al., 2006; Mohanty et al., 1996). Along with sea surface temperature (SST), anomalies modulate various atmospheric fields and influence the intensity and propagation of Indian summer monsoon (ISM) circulation (Jalihal et al., 2019; Johari, 2020). Numerous studies have highlighted the long-term and seasonal variability of surface heat fluxes over the global oceans and their direct association with monsoon dynamics (Weare et al., 1981; Bollasina and Ming, 2013; Bhatla et al., 2016). Regional changes in the energy balance influence the pressure gradient between land and ocean, which in turn governs wind patterns, moisture transport, local convection, and ultimately the distribution of monsoonal rainfall (Turner and Annamalai,

* Corresponding author. Department of Geophysics, Institute of Science, Banaras Hindu University, Varanasi, 221005, U.P. India.
E-mail address: rbhatla@bhu.ac.in (R. Bhatla).

https://doi.org/10.1016/j.jastp.2025.106568
Received 1 January 2025; Received in revised form 13 June 2025; Accepted 14 June 2025
Available online 20 June 2025

2012; Trenberth and Guillemot, 1998). Therefore the ISM is a complex meteorological phenomenon influenced by a range of factors, including surface energy fluxes and radiative forcing (Bhatla et al., 2011; Mohanty et al., 2019). The four key components of the surface energy balance crucial to the Indian monsoon system are latent heat flux (LHF), sensible heat flux (SHF), net incoming shortwave radiation flux (NSW), and net outgoing longwave radiation flux (NLW). LHF plays a critical role in the energy balance of the monsoon system. The changes in surface LHF and SHF between the ocean and land significantly affect the low-level monsoonal circulation in the tropics (Wang and Wu, 2008). Regarding surface heat fluxes, a definite coupling exists between the land surface and the atmosphere, which leads to convection activities (Yang et al., 2020). The intense moisture transfer in the near-surface atmosphere causes enhanced convective precipitation and is significantly associated with surface heat fluxes (Trenberth et al., 2009; Webster, 1994). In the past few decades, significant surface cooling (warming) trends over the Tibetan plateau, East Asia, and the tropical Indian region have been reported (Folland et al., 2001; Hu and Duan, 2015). The changes in surface fluxes over the Indian region seem to directly influence the moisture budget during ISM season (Goswami and Chakravorty, 2017) by altering the convective activities and modulating the monsoon circulation over the Indian subcontinent and adjoining region. The ISMR primarily impacts agricultural production and directly or indirectly affects the Indian economy. Thus, it is essential to unravel the vagaries of monsoon to understand the variation of surface fluxes and impacts on the dynamics of ISMR under changing climate.

The changes in land use, atmospheric greenhouse gas concentrations, and other factors can lead to changes in the surface energy balance and radiative forcing, which can in turn affect the dynamics of ISM season. The Earth's climate has changed dramatically on a global and regional scale during the last ten decades due to global warming (IPCC, 2013). Several authors have found significant projected changes in ISMR patterns and related extremes over Indian regions under warming scenarios (Sharmila et al., 2015; Pant et al., 2023; Verma et al., 2023). The combined contribution of the anthropogenic effect and the robust internal mode climate system is responsible for this transformation (Trenberth et al., 2003). The natural climatic indices like El-Nino Southern Oscillation (ENSO), Pacific Decadal Oscillation (PDO), and Atlantic Multi-decadal Oscillation (AMO) have a significant influence on global and regional average temperature and rainfall (Krishnamurthy and Krishnamurthy, 2014; Malik et al., 2017; Chang et al., 2019; Roy et al., 2019).

Therefore, this study demonstrates the climatological, tricadal, and decadal variability of surface energy fluxes and their association with the Indian Summer Monsoon. The analysis identifies the spatial and temporal pattern characteristics of possible physical significance. In addition, this study focuses on planetary-scale thermal and dynamical attributes of the atmosphere over the study domain. It also contributes to the United Nations Sustainable Development Goals (UN SDGs), particularly SDG 13 (Climate Action), SDG 2 (Zero Hunger), and SDG 6 (Clean Water and Sanitation). By examining long-term shifts in surface energy fluxes and monsoon dynamics, the findings support climate-resilient planning for agriculture and water resources in monsoon-dependent regions like India. As highlighted by Varotsos and Cracknell (2020), climate-related research plays a crucial role in advancing global sustainability targets by informing adaptation and mitigation strategies. The following section provides a brief description of the datasets used in this study, followed by the data and methodology outlined in Section 2. Section 3 presents the epochal variations in rainfall and surface fluxes, along with their association with the Indian Summer Monsoon under a changing climate. Finally, Section 4 summarizes the key findings and conclusions of the study.

2. Data and methodology

The monthly mean gridded rainfall data over the Indian region at a resolution of 0.25° × 0.25° is available from the India Meteorological Department (Pai et al., 2014) and has been considered for the June, July, August and September (JJAS or ISMR season) during the period 1961–2020. The European Centre for Medium-Range Weather Forecasts (ECMWF) developed the latest atmospheric reanalysis, known as the fifth-generation climate reanalysis (ERA5), which has a high spatial resolution of 0.25° × 0.25°. This data can be accessed through the Climate Data Service portal (https://cds.climate.copernicus.eu/). The ERA5 reanalysis datasets are widely used for hydroclimatic applications and are the most suitable for representing the annual and seasonal climatological averages globally (Albergel et al., 2018; Hersbach et al., 2018). Furthermore, this study utilizes the 60-year (1961–2020) daily reanalysis data from the National Centers for Environmental Prediction (NCEP) and the National Center for Atmospheric Research (NCAR), which has a horizontal resolution of 2.5° × 2.5°. This dataset offers a consistent and reliable resource for examining the variation of energy fluxes during the Indian Summer Monsoon Rainfall (ISMR) season (Kalnay et al., 1996). The NCEP reanalysis data plays a vital role in understanding the climate system and also helps in examining the variation of derived meteorological parameters during ISM over the Indian region (40° N-30°S & 30°E-110°E) and is freely available at http://www.cdc.noaa.gov/cdc/data.ncep.reanalysis.surface.html. These datasets have been used in several spatiotemporal climate studies (Leetmaa et al., 1996; Yanai and Tomita, 1998; Bhatla et al., 2022; Maurya et al., 2023). The mean daily reanalysis basic and derived parameters have been *considered* for the period 1961–2020. Further, the long-term surface fluxes, dynamic and thermodynamic features, and moisture flux are studied during ISM season. The spatial variation of derived meteorological parameters (energy fluxes) shows epochal changes in long-term tricadal and decadal anomalies. The various quantities have been computed as follows:

Net heat flux (NHF): NHF is calculated using the formula:

$$\boldsymbol{NHF} = \boldsymbol{NSW} - (\boldsymbol{NLW} + \boldsymbol{LHF} + \boldsymbol{SHF}) \quad (1)$$

Where, NSW is the net incoming shortwave radiation, NLW is the net outgoing longwave radiation, LHF is latent heat flux, and SHF is sensible heat flux.

Empirical orthogonal function (EOF) analysis is often used to study possible spatial patterns of climate variability and how they change with time. Therefore, EOFs of a space-time physical process can represent mutually orthogonal space patterns where the data variance is concentrated, with the first pattern being responsible for the most significant part of the variance (Barnett, 1978; Dai et al., 2015; Singh, 2004).

2.1. Moist static energy (MSE)

The atmospheric thermodynamic feature is defined by MSE as the sum of internal, potential, and moist energy. It has been widely used in tropical regions because of its energetic and conventionally recognised conservation properties (Fontaine et al., 1999), and is mathematically written as:

$$\mathrm{MSE} = \mathrm{CpT} + \mathrm{gz} + \mathrm{Lv\ q} \quad (2)$$

W*here*, Cp is the specific heat capacity at constant pressure (1004 JK-1Kg-1), T is temperature, g is the gravitational acceleration (9.8ms-2), z is the geopotential height, Lv is the latent heat of vaporisation (2.5 × 106JKg-1), and q is the specific humidity.

2.2. Moisture flux convergence (MFC)

MFC is the sum of moisture advection and convection (Banacos and Schultz, 2005) and is mathematically written as:

$$MFC = MFC_{advect} + MFC_{conv} \quad (3)$$

Where, $MFC_{advect} = -$ and $MFC_{conv} = -q\left(\left(\frac{du}{dx}\right) + \left(\frac{dv}{dy}\right)\right)$; u is the zonal wind, v is meridional wind, q is specific humidity, x and y are the latitude and longitude.

2.3. Moisture flux (MF) and vertically integrated moisture flux convergence (VIMFC)

Moisture Flux (MF) is the multiplication of specific humidity and wind (Where; $q \times u =$ Zonal moisture flux & $q \times v =$ Meridional moisture flux).

The formulation of VIMFC follows Trenberth and Guillemot (1998) and is expressed as:

$$\text{VIMFC} = -\nabla.\frac{1}{g}\int_{ps}^{p} qVdp \tag{4}$$

Where, V is wind vector velocity, ∇ is the gradient operator, and is integrated over the surface (1000 hPa) to the top of the atmosphere (300 hPa) concerning pressure.

As suggested by Fasullo and Webster (2003) and Kalnay et al. (1996) regarding the VIMFC above 300 hPa, the specific humidity has a negligible impact on the calculation of total vertically integrated moisture transport above this level and is not part of the reanalysis. Seasonal

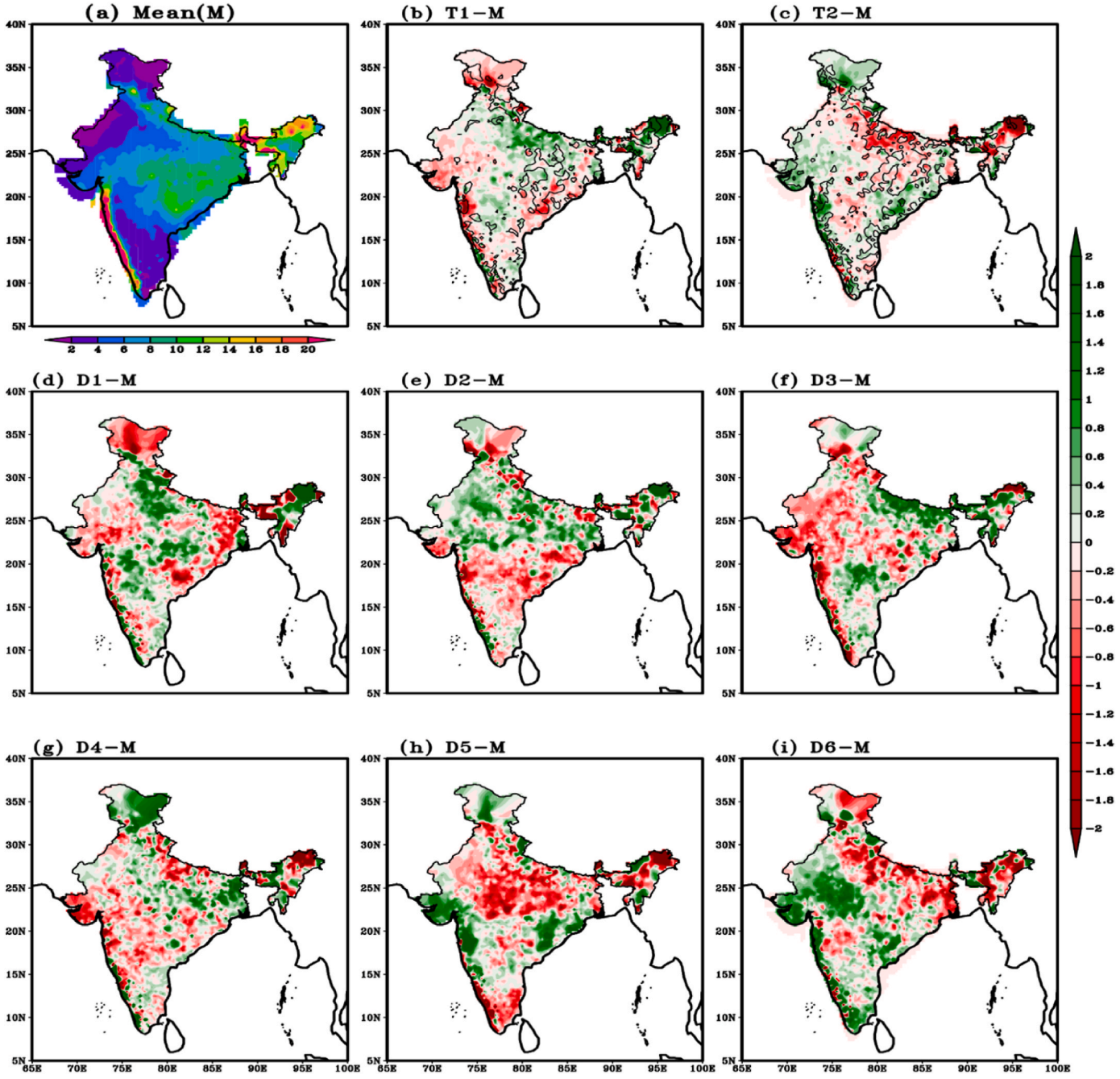

Fig. 1. (a–i): The climatological and epochal distribution of precipitation (mm/day) using IMD datasets during June–September (JJAS) for (a) 1961–2020 (Mean distribution of rainfall (M)); (b) Past tricadal difference from mean distribution of precipitation; (c) recent tricade difference from mean (Past tricade: T1; 1961–1990), (recent tricade: T2; 1991–2000); (d)–(i) decadal differences from the mean (M), first decade (D1; 1961–1970); second (D2; 1971–1980) third (D3; 1981–1990), fourth (D4; 1991–2000), fifth (D5; 2001–2010), sixth (D6; 2011–2020), decades respectively. The regions with 95 % confidence level are contoured.

and spatial variations in different fluxes play a significant role during the ISM season. The large-scale circulation of SST, wind, surface fluxes, and dynamic as well as thermodynamic features are briefly presented to show an overview of these factors over the Indian monsoon domain and its adjoining areas. Here, other changes of epochal distribution with average (Climatology; 1961–2020), two tricades (T1; 1961–1990; T2; 1991–2020) and six decades (D1; 1961–1970, D2; 1971–1980, D3; 1981–1990, D4; 1991–2000, D5; 2001–2010, D6; 2011–2020) have been discussed. Anomalies are presented with respect to the long-term climatology (1961–2020), rather than through direct epoch-to-epoch differences (e.g., T2–T1 or D6–D1). This approach is intentionally adopted to provide a stable and consistent baseline that captures systematic deviations in surface fluxes and related parameters over multiple decades. Using climatological baselines (T1–M, D1–M, etc.) helps reduce the impact of short-term or arbitrary fluctuations that may arise when only two epochs are directly compared. This method is widely used in observational climate studies to extract low-frequency variability and long-term signals in atmospheric diagnostics (Meehl and Hu, 2006). Supplementary comparisons such as T2–T1 are also included for reference. In addition, the student's t-test is used to determine significance at 95 % in the past and recent tricadal differences with long-term climatology for the considered period.

3. Results and analysis

3.1. Spatio-temporal distribution patterns of basic meteorological variables during ISM season

The spatio-temporal distribution of mean ISMR and variations for tricadal and decadal timescales have been illustrated in Fig. 1 with observations (IMD) and ERA5 reanalysis data. The maximum rainfall has been perceived along the Western Ghats (WGs) and north-eastern India (NEI) (16–20 mm/day). Central India (CI), Northern India (NI), and its adjoining region have also experienced considerable rainfall of the order of 8–12 mm/day (Fig. 1a). The past and recent tricadal difference from seasonal mean rainfall is depicted in Fig. 1b and c. In the past tricade, the rainfall departure from climatology has highlighted regions with excess or wet rainfall, such as the Upper Gangetic Plain, Lower West Bengal, and the northern and eastern parts (with departures ranging from 1 to 2 mm/day; Fig. 1b). In contrast, rain-deficient or dry areas include Northwest India, the Upper Western Ghats, Eastern Peninsular India, and the northernmost parts of India, with departures ranging from −0.6 to −1.5 mm/day. On the contrary, a dominant significant contrasting pattern has been observed in recent tricade departure (Fig. 1c). Positive differences have been observed over Western India (WI), some parts of WGs, NI, and the central NEI region at 95 % confidence level. The recent decadal pattern demonstrates a positive rainfall anomaly (0.8–2 mm/day) over WI, some parts of CI, southern peninsular India (SPI), and the hilly region. In contrast, negative anomalies have been found over the NEI and Gangetic-plain regions, possibly due to the anomalous changing pattern of land ocean thermal contrast in warming climate. Similarly, the spatial distribution of ISMR derived from ERA5 reanalysis over land and ocean regions is shown in Fig. 2a–i. A significant difference in tricades and decades with long-term climatology has been noticed. However, tricadal changes in the ERA5 data are inconsistent with observations. However, it can highlight the significant regions that followed the oscillation patterns in positive and negative differences from south to north in tricadal and decadal differences. In the recent decade (Fig. 2i), a positive anomaly has been observed over the western Equatorial Indian Ocean (EIO), northern Arabian Sea (AS), southern Bay of Bengal (BoB), WGs, SPI and some parts of central NEI whereas negative differences have been seen over northern EIO, northern BoB, NEI. A significant increase (decrease) in the spatial extent of rainfall is visible. The recent tricade and decades present the anomalous decrease in monsoon rainfall that might be associated with the warming of the Indian Ocean (Roxy et al., 2015; Goswami, 2023). While ERA5 and IMD datasets capture broadly similar rainfall distributions, notable discrepancies emerge in their tricadal and decadal differences. These differences are expected and stem from the nature of the datasets: IMD is purely observational and station-based, while ERA5 is a physically constrained reanalysis product that assimilates model outputs with observations. Such disagreements do not undermine the results; rather, they emphasize the importance of using multiple independent datasets for cross-validation. The regions where ERA5 and IMD diverge, particularly in NEI and over the oceanic sectors offer: valuable insight into the limitations and strengths of each dataset. ERA5 helps extend spatial coverage and provides atmospheric consistency across variables, while IMD retains high fidelity in densely observed land regions. These differences have been explicitly considered while interpreting rainfall trends and surface flux variability.

The spatial patterns of SST and wind anomalies during different epochs (Fig. 3a–i) reveal substantial warming of the Indian Ocean, especially over the western EIO and northern AS during the recent decade. This enhanced SST gradient intensifies the zonal and meridional moisture flux, particularly northward from the equator into the AS. Such SST-induced convergence zones over the AS and BoB modulate monsoon winds, promoting enhanced convection in certain regions. This mechanism is consistent with previous findings that link basin-wide Indian Ocean warming to monsoon variability through the modulation of moisture convergence and atmospheric instability (Roxy et al., 2015). The observed SST warming creates favourable large-scale thermodynamic conditions that may support monsoon recovery in specific subregions, though it may also suppress rainfall in others due to altered convection zones. These regional responses depend on the location of maximum SST anomaly and associated wind convergence.

3.2. Spatio-temporal variation in surface fluxes during ISM season

The warming sea surface plays a vital role in linking the ocean and the atmosphere and, consequently, in generating clouds. The spatio-temporal distribution and variation in NSW have been illustrated in Fig. 4a–i. The negative sign indicates the direction of incoming solar radiation, which has been corrected for the calculation of tricadal and decadal differences in the Net Heat Flux (NHF). The maximum NSW is observed over land regions, the eastern and western IO, and the AS, ranging between 180 and 200 W/m^2. The minimum values are found over the Southern Indian Ocean (SIO) and the BoB and its adjoining regions, with values in the range of 140–180 W/m^2. These variations are attributed to the presence of cloud cover and the movement of the ITCZ (Fig. 4a). A contrasting pattern of NSW over land and oceanic regions has been reported during the recent tricade (T2) as compared with the previous one (T1) (Fig. 4 b&c). In past tricadal anomaly (T1-M), a positive difference (2–6 W/m^2) is observed over eastern AS (EAS), BoB, SPI, and WI. In contrast, a negative anomaly (−1 to −10 W/m^2) is observed over eastern and western EIO, western AS (WAS), SIO, NI and NEI regions with significance at a 95 % confidence level. However, a significant enhancement (1–6 W/m^2) in NSW has been found over SIO, eastern and western EIO, WAS, NI, and NEI regions. On the other hand, a decrease anomaly was observed over the SPI, WI, EAS, and BoB regions (−3 to −10 W/m^2) during the recent tricade compared to mean patterns. Similarly, the decadal differences from the mean climatology of NSW have been shown in Fig. 4d–i. Significant variations are observed over different regions from past to recent decades. Along with the recent decadal anomaly, the spatiotemporal distribution of NSW over the NE, the adjoining region, and lower SIO, EIO, and WAS have an increasing pattern (2–10 W/m^2). In contrast, a decrease over the BoB, EAS, SPI, WI, and NI in the −1 to −10 W/m^2 range has been noticed. Further, the southern BoB has significantly more negative NSW than the rest of India (−4 to −12 W/m^2). It is observed that the variation of NSW has increased substantially over NE and its adjoining region, as well as WAS and western EIO. Conversely, a decreasing pattern has been observed in the recent decade over the SPI, EAS, and BoB regions.

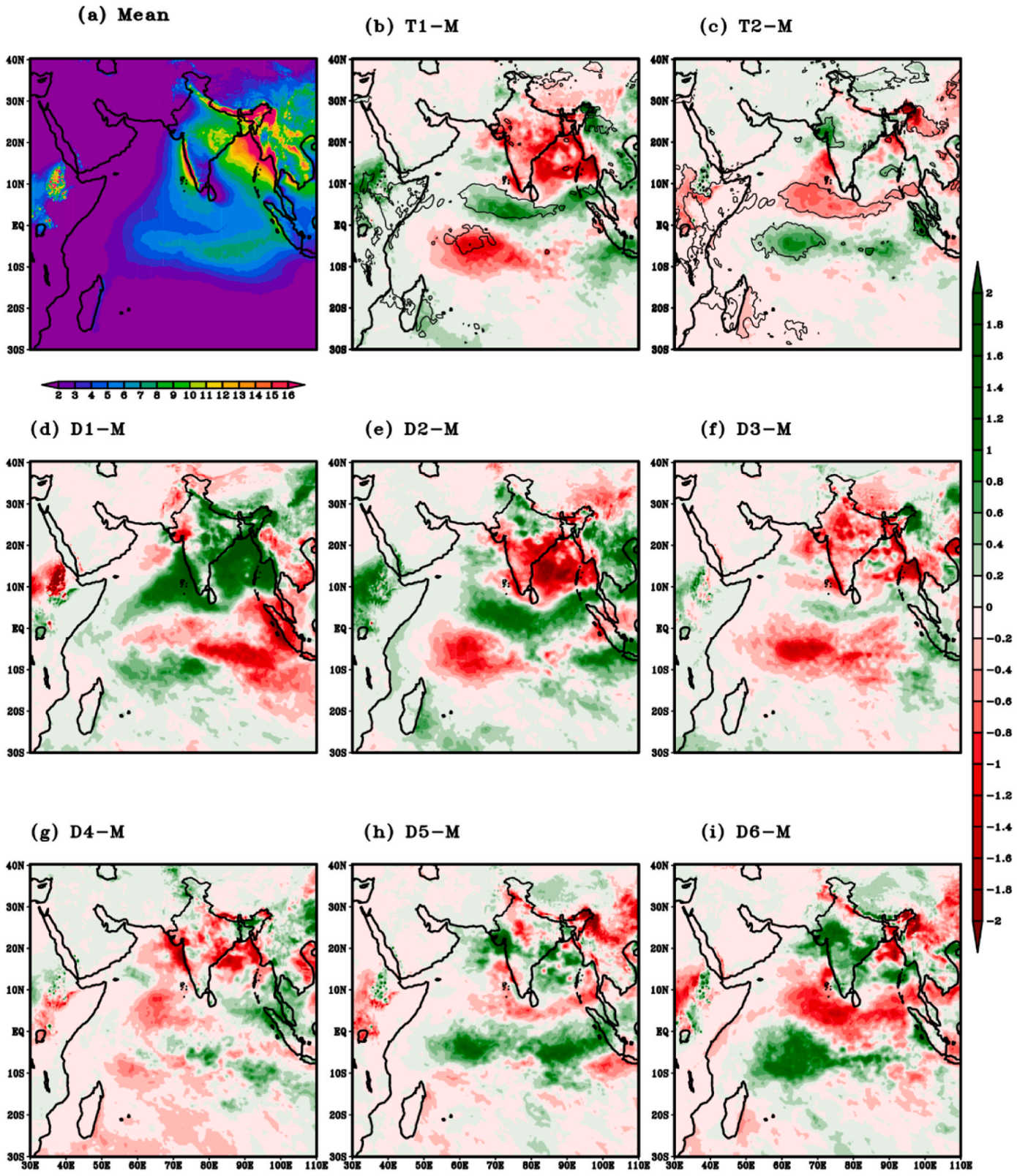

Fig. 2. (a–i): The climatological and epochal distribution of precipitation (mm/day) from ERA5 datasets during June–September (JJAS) for (a) 1961–2020 (Mean distribution of rainfall (M)); (b) Past tricadal difference from mean distribution of precipitation; (c) recent tricade difference from mean (Past tricade: T1; 1961–1990), (recent tricade: T2; 1991–2000); (d)–(i) decadal differences from the mean (M), first decade (D1; 1961–1970); second (D2; 1971–1980) third (D3; 1981–1990), fourth (D4; 1991–2000), fifth (D5; 2001–2010), sixth (D6; 2011–2020), decades respectively. The regions with 95 % confidence level are contoured.

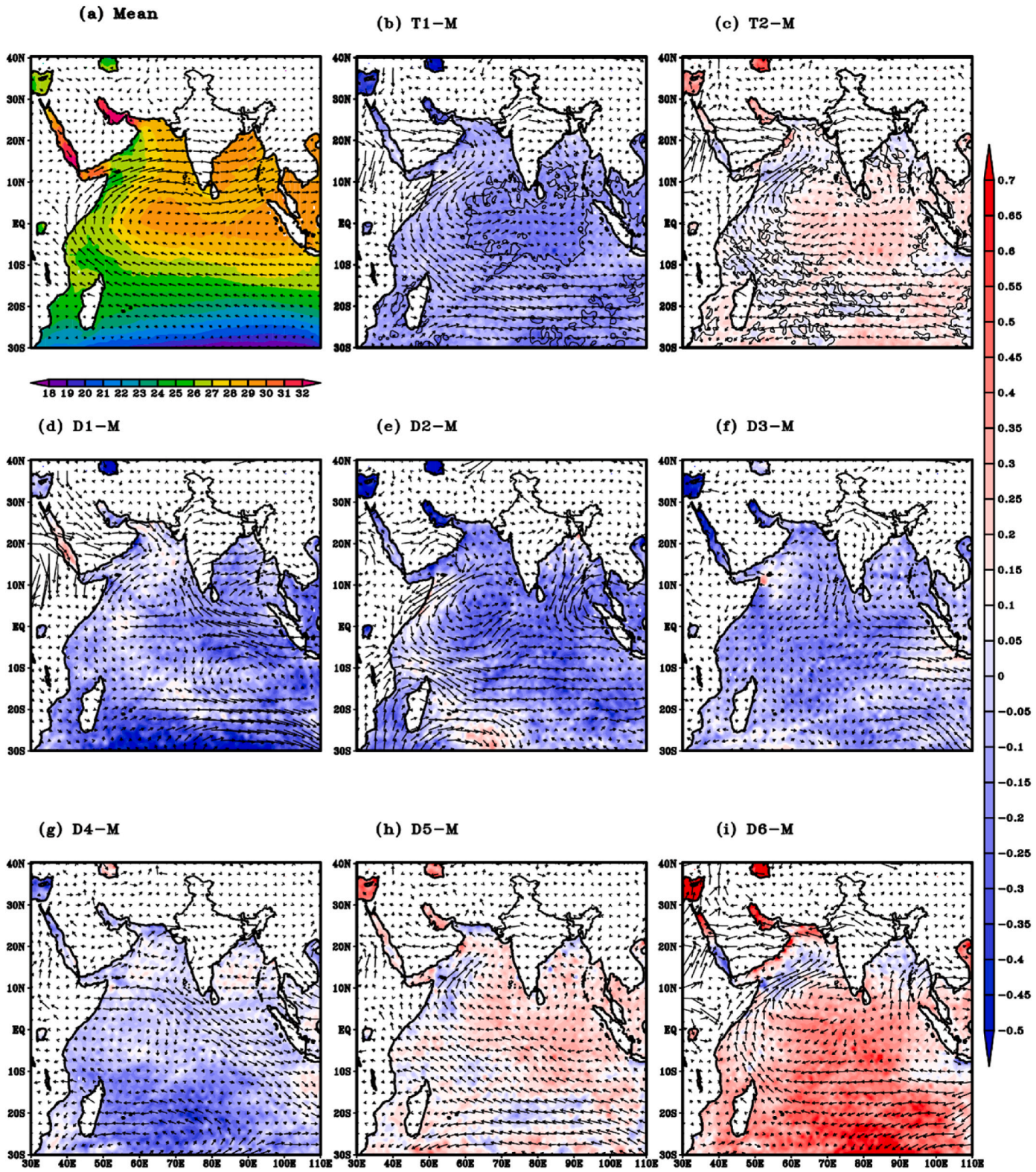

Fig. 3. (a–i): Same as Fig. 1, but for sea surface temperature (m/s) at 850 hpa for JJAS in shaded and wind vector (m/s) at 850 hpa for JJAS.

LHF is the most essential component of the convection system (Liu and Curry, 2006; Wu et al., 2020). The variation in the LHF explains the large amplitude of interannual and spatial variability in the global climate system. The distribution of surface LHF climatology during ISM season, along with tricadal and decadal differences, has been illustrated in Fig. 5a–i. The maximum surface LHF (180–210 W/m^2) is found over the SIO, BoB, and AS during the considered period of average climatology and is depicted in Fig. 5a. Along with this, some parts of WGs have more LHF (120–150 W/m^2) than all India regions (80–120 W/m^2), further decreasing over WI, some parts of NEI, and adjoining regions of NWI (30–60 W/m^2). The regions within the rectangles have shown higher values of LHF and follow a similar part for the maximum

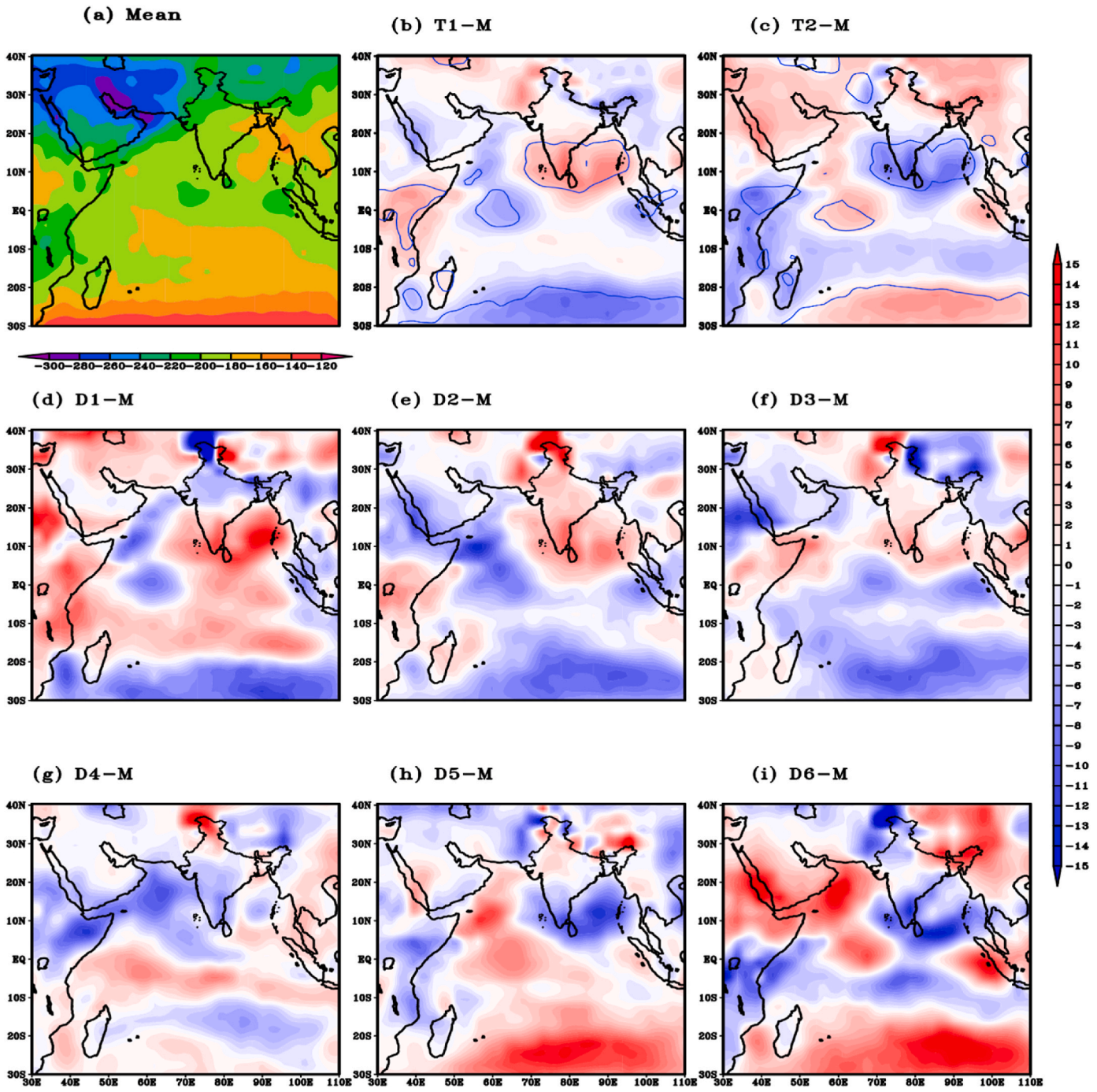

Fig. 4. (a–i): Same as Fig. 1, but for net incoming shortwave radiation flux (NSW; W/m^2) for JJAS.

variability in surface temperature and precipitation in the findings of Bhatla et al. (2022) (Table 1). A contrasting pattern of LHF changes has been observed over the oceanic region during the considered tricadal periods, and the differences are significant at 95 % level (Fig. 5b and c). The study by Zeng and Zhang (2020) explained that variation in LHF during the ISM season is dominated over the oceanic regions rather than the land due to the higher heat capacity of water. The decadal differences also depicted the significantly increasing and decreasing pattern of LHF over the oceanic and land regions. During the last decade, the decreasing pattern of LHF over central SIO, AS, and BoB (−2 to −12 W/m^2) and increased pattern of LHF (2–14 W/m^2) observed over EIO, some parts of WI, NI, and SPI regions has been found during the recent decade (Fig. 5i). The NHF is defined as the balance between incoming and outgoing energy flux in the atmosphere, all available energy affects the climate. The NHF radiation is the difference between total incoming and total outgoing radiation (net outgoing longwave radiation + latent heat + sensible heat). The NSW and LHF contribute significantly to the variation of NHF over the oceanic regions. The long-term NHF distribution pattern or climatology, tricadal, and decadal differences from the climatology are shown in Fig. 6a–i. A positive NHF value denotes higher incoming energy than outgoing, while a negative value denotes lesser incoming and higher outgoing energy. The negative NHF pattern has been observed over most oceanic regions, such as AS, BoB and SIO, with a variation of −20 to −80 W/m$^{2.}$ In contrast, slightly positive values (10–40 W/m^2) can be noticed over Indian landmass, especially over CI regions along with some northern BoB and northern AS regions (Fig. 6a).

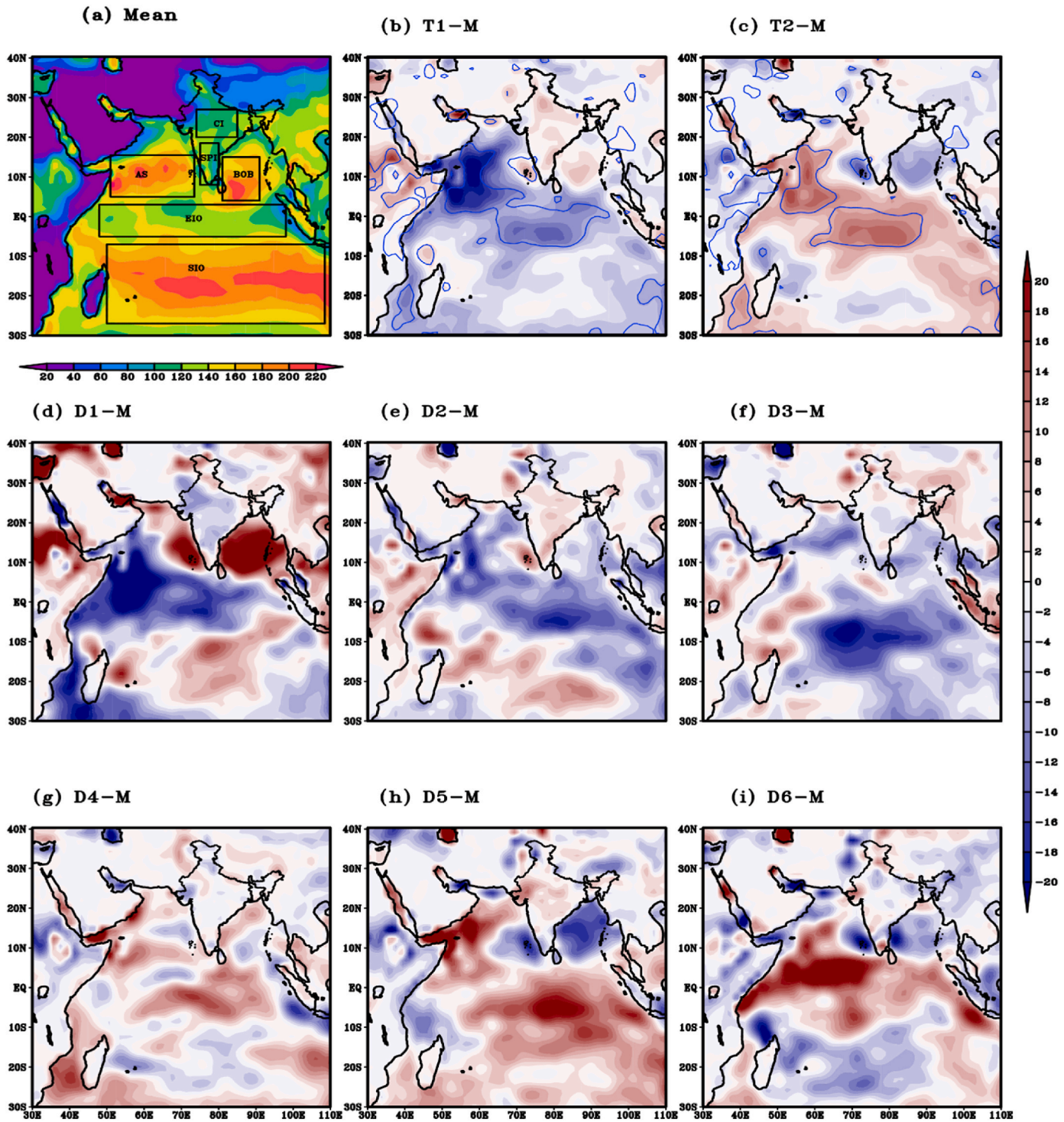

Fig. 5. (a–i): Same as Fig. 1, but for surface latent heat flux (LHF; W/m^2).

Table 1
List of selected regions.

Sr. No.	Regions	Lat/Lon
1.	*Central India (CI)*	74-85°E, 20–27°N
2.	*Southern Peninsular India (SPI)*	75-80°E, 8–18.5°N
3.	*Arabian Sea (AS)*	51–73.5°E, 5–15°N
4.	*Bay of Bengal (BoB)*	81-91°E, 4–15°N
5.	*Equatorial Indian Ocean (EIO)*	48-98°E, 5°S-3°N
6.	*Southern Indian Ocean (SIO)*	50–108.5°E, 28.5°S-5°S

The negative anomalies are mainly attributed to strong low-level wind and enhanced evaporation, leading to upwelling, cooling of the sea surface, and enhanced monsoon convective activity with more cloud cover and reduction of incoming short-wave radiation (Mohanty et al., 1994). Further, the anomalous patterns of NHF show positive values (2–15 W/m^2) over AS and BoB regions while larger negative values (−5 to −15 W/m^2) over the EIO and WAS during the recent tricade and decade. A closure encounter on the recent tricadal and decadal anomalies (Fig. 6b–i) reveals an increment in negative NHF over EIO and WAS. In contrast, positive NHF over the EAS and southern BoB has been

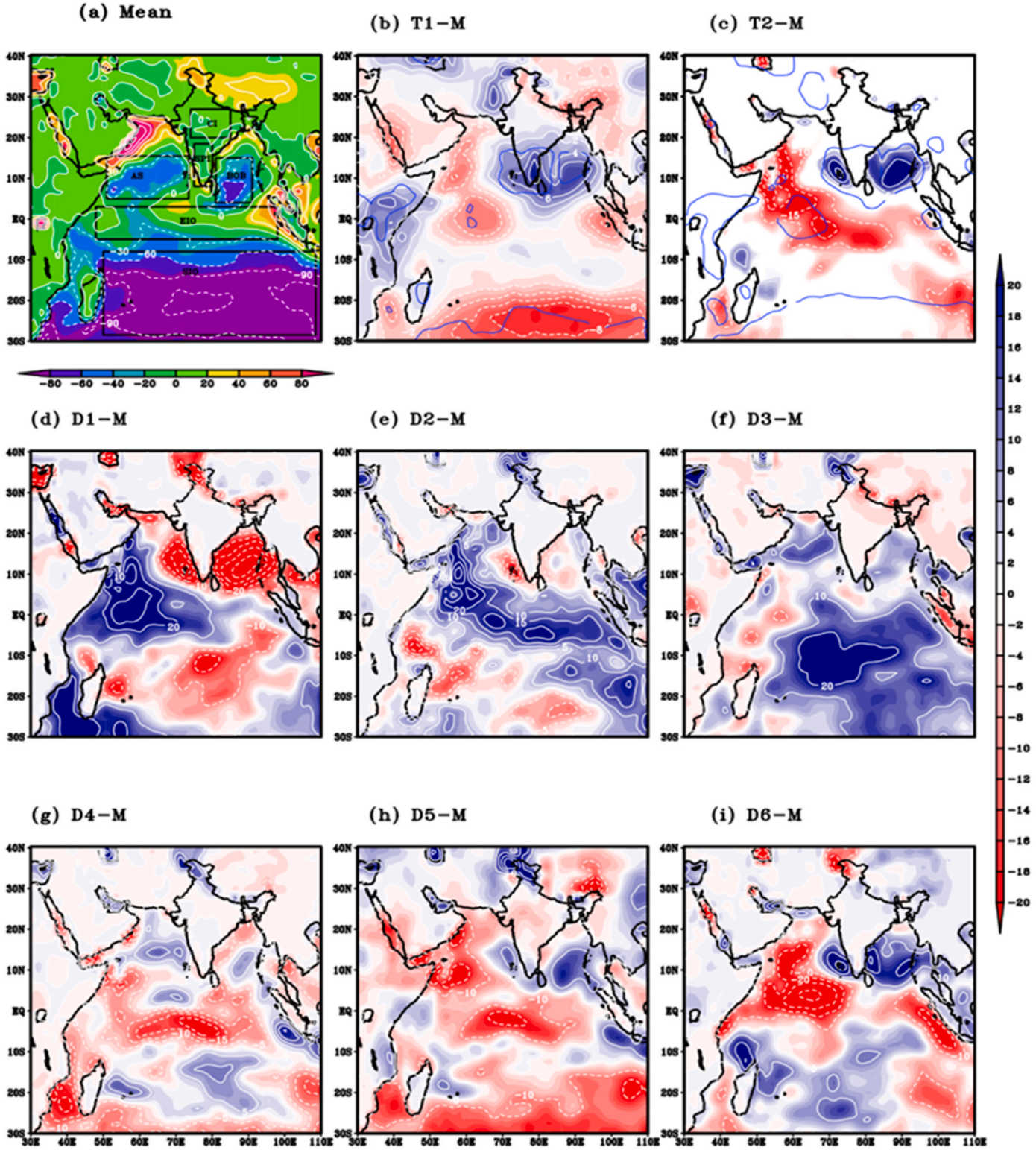

Fig. 6. (a–i): Same as Fig. 1, but for net heat flux (NHF; W/m^2).

observed, possibly due to the more convective heating over the region.

3.3. Tricadal differences of surface energy fluxes during ISM season over different regions

This section explores the tricadal differences in energy fluxes over the land and oceanic regions and their influences during the ISMR season. The tricadal differences (T2-T1) of surface fluxes over different selected regions based on the variability of LHF and NHF have been illustrated in Fig. 7. There are significant positive variations in NSW observed over the SPI and BoB region in the order of 13–14 W/m^2, whereas negative anomalies have been observed over the SIO region (−10 W/m^2). Higher positive changes in LHF are depicted over AS and EIO regions (10–12 W/m^2), whereas the BoB region has been shown to

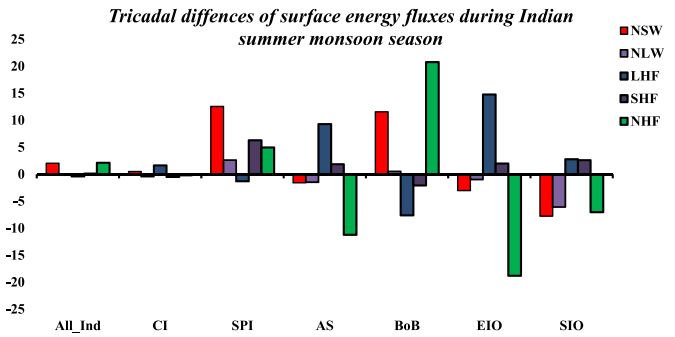

Fig. 7. Tricadal differences of surface energy fluxes during ISMR over different regions All_Ind; all India and its adjoining region, CI: Central India, SPI: Southern Peninsular India; AS: Arabian Sea; BoB: Bay of Bengal; EIO: equatorial Indian region; SIO: southern Indian Ocean.

have negative differences (−8 W/m^2). It means that in the recent tricade, LHF has decreased in comparison to the past tricade over the BoB region, while it has increased over the AS and EIO region during the ISMR season. On the other hand, NHF has a negative variation over AS, EIO, and SIO. In contrast, a positive difference has been observed over the BoB region due to positive NSW and negative LHF. Sensible heat flux has less anomaly overall except for SPI. The primary significant changes of surface fluxes over SPI (NSW, SHF, NHF), AS (LHF, NHF), BoB (NSW, LHF, NHF), EIO (LHF, NHF), SIO (NSW, NLW, NHF), and also justify the pattern observed in Figss. 4–6. The enhanced surface fluxes increase precipitation, and the latent heat release most likely causes the circulation alterations. Deshpande and Kulkarni (2022), recently reported that tricadal differences in surface fluxes over different regions show more variation in convective heating and give convective precipitation with stratiform clouds. The large-scale dynamics parameterisation also suggests that convective precipitation responds extremely strongly to surface turbulent heat fluxes (Chakraborty et al., 2015).

3.4. Leading mode of variability in surface fluxes and its association with ISMR

The leading EOF modes for the surface fluxes (NSW, LHF & NHF) using reanalysis datasets are analysed over the ISM domain of 30°S–40°N, 30°E−110° for the extended period 1961–2020 (Fig. 8a–i). The EOF analysis applied to the surface flux datasets reveals three dominant modes (EOF1, EOF2 & EOF3) of variability, explaining 26.41 %, 14.77 % and 11.05 % of the total variance for NSW, 28.4 %, 18.27 % and 11.37 % for LHF and 21.4 %, 19.24 %, 12.08 % for NHF respectively. The pattern, NSW_EOF1 (Fig. 8a), having most of its amplitude over the EAS, BoB, EIO, SPI, CI, WI, and NI, shows a positive anomaly and a strong negative anomaly over eastern SIO, some parts of east and WEIO, WAS and NEI regions. Further, the second pattern, i.e., NSW_EOF2 (Fig. 8b), has a strong negative anomaly over the AS and SPI region. In contrast, a weak negative anomaly has been observed over almost the entire Indian landmass and oceanic region except for some parts of SIO and NI. In the third pattern, NSW_EOF3 (Fig. 8c), slightly negative anomalies have been observed over the entire region except for NI. The temporal modulation effect of the land and ocean interaction surface is studied by considering the time characteristics of the first, second, and third principal components PCl, PC2, and PC3 (Fig. 9a–c). The time series of the PCl, PC2, and PC3 indicates that the dominant mode mainly describes the epochal behaviour of the ISM in changing climate and agrees with the results of Annamalai et al. (1999). The anomalous increasing value of LHF over AS and BoB is explained by the second dominant mode of EOF2 and PC2; after 1975, PC2 of the LHF became dominant over PC1.

3.5. Spatiotemporal variation of dynamic and thermodynamic components during ISM season

An essential parameter for assessing atmospheric thermodynamic conditions is the MSE. The spatial variation of mean MSE with tricadal anomalies at 850 hPa has been depicted in Fig. 10a–c. The spatial distribution of mean climatology has a broader belt structure of lower MSE (308–320 kJ/kg) over the SIO region. Higher values of MSE can be seen over the land regions due to more diabatic heating over land. The maximum variation of MSE is found over land (NI, CI, WI, Himalayan region, and TP) and some parts of the oceanic regions such as AS and BoB. From Fig. 10b and c, it is clear that the past tricadal anomalies of MSE contrast with the recent tricade over land and oceanic regions. Further, in the recent tricadal anomaly (T2-M), a significantly increasing pattern of MSE was observed over SIO, AS, BoB, and Indian landmass regions. Contrary to that, a minimum amount of MSE (−0.25 to −0.75 kJ/kg) has been reported over the eastern part of SIO and the western part of AS. In the recent warming period, the MSE increased support towards escalating monsoon convective activity over this region. It is interesting to notice that the MSE has increased along the entire longitude of the NI region, maximising around the longitude of WI, indicating an increase in the convective activity. MSE and wind distributions confirm the increasing convective activity, particularly over WI in the recent warming period. The rising atmospheric moisture due to the increased moisture transport and the favourable convective condition has increased rainfall over some parts of WI during the ISM season. These changes in atmospheric dynamics in the recent warming period may lead to possible greening of the desert if favourable atmospheric conditions conducive to rainfall persist for a longer time. When the MSE is higher, more energy is available to lift moisture upwards, leading to condensation, precipitation, and ultimately, vertical motions associated with the atmospheric circulation. On the other hand, it is discovered that longwave radiative heating keeps the MSE anomalies from dissipating due to horizontal MSE advection (Sooraj and Seo, 2013). Due to the vertical motion caused by anomalous heating, more water vapour is available for precipitation anomalies (Huo et al., 2022).

Moisture flux convergence (MFC) is the crucial factor for determining atmospheric stability and is discussed in the methodology section by equation (3). MFC is often used as a diagnostic tool to understand the dynamics of monsoon systems. The spatiotemporal distribution of MFC has been depicted in Fig. 10d–f with mean, tricadal differences during ISM season. From Fig. 10d–f, a positive MFC value represents convergence, whereas a negative MFC value represents divergence. During the monsoon season, warm and moist air from the ocean to the landmass converges with cooler and drier air over the land. Several factors, such as low-level jets, land-sea breeze circulations, and topographical features, enhance the moisture flux convergence. This convergence of air masses leads to the formation of convective clouds and precipitation. The contrasting patterns of MFC have been observed in past and recent tricadal variations such as precipitation, SST, and surface fluxes. Over some parts of India and adjoining regions, it has been observed that MFC follows patterns that are almost similar to rainfall and wind patterns. This suggests that convection over these regions may be explained with MFC and favouring the formation of deep convective clouds (Adames and Ming, 2018; Karmakar and Misra, 2020). Understanding the moisture flux convergence patterns during the monsoon season is crucial for managing water resources, agriculture, and other aspects of human life in affected regions.

The MF and VIMFC of u and v components averaged from 1961 to 2020 (1000–300 hPa) have been shown in Fig. 10g–i. In this figure, the moisture transport appears from the south-westerly direction, with strong moisture from the IO during the ISM season. The moisture transport is most substantial with the VIMFC over EIO, AS, BoB and significant parts of the SPI region. This moisture transports from the IO towards the land region and may bring more rainfall over India and the adjoining region. The VIMFC provides a valuable measure of the tropical

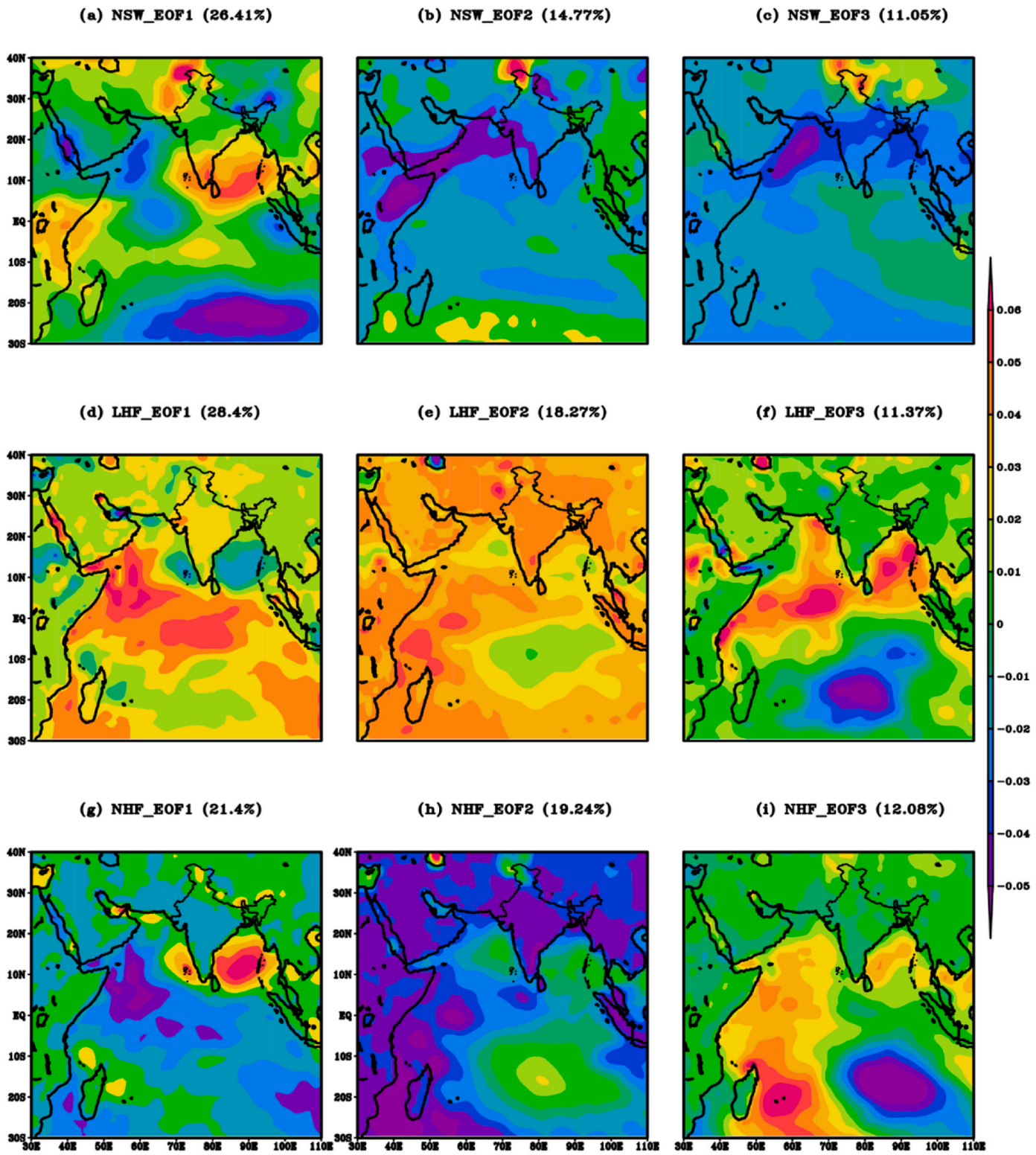

Fig. 8. (a–i): Spatial pattern of the three modes of EOF surface fluxes Net incoming short wave radiation flux (NSW), Latent heat flux (LHF) and Net heat flux (NHF) over the Indian region and its adjoining region during Indian summer monsoon season for the period of 1961–2020, and (a–c) first, second and third EOF mode for the NSW (d–e) is same as (a–c), but for the LHF. (g–i) is the same as (a–c), but for the NHF.

atmospheric hydrological cycle and reflects the combined dynamical and thermodynamical effects. In the spatial distribution of MF with VIMFC during past and recent tricadal anomalies, contrasting patterns are observed. In the recent tricadal anomaly, a decreasing pattern has been observed over the western EIO, EAS, WI, CI, and NEI region and is statistically significant at a 95 % confidence level. Since the ISM season is sustained by a continuous supply of moisture from the IO. However, moisture convergence and severe diabatic heating are essential for maintaining monsoonal circulation (Rao and Reddy, 2019; Krishnamurti and Sikka, 1978). However, the moisture flux analysis was even more

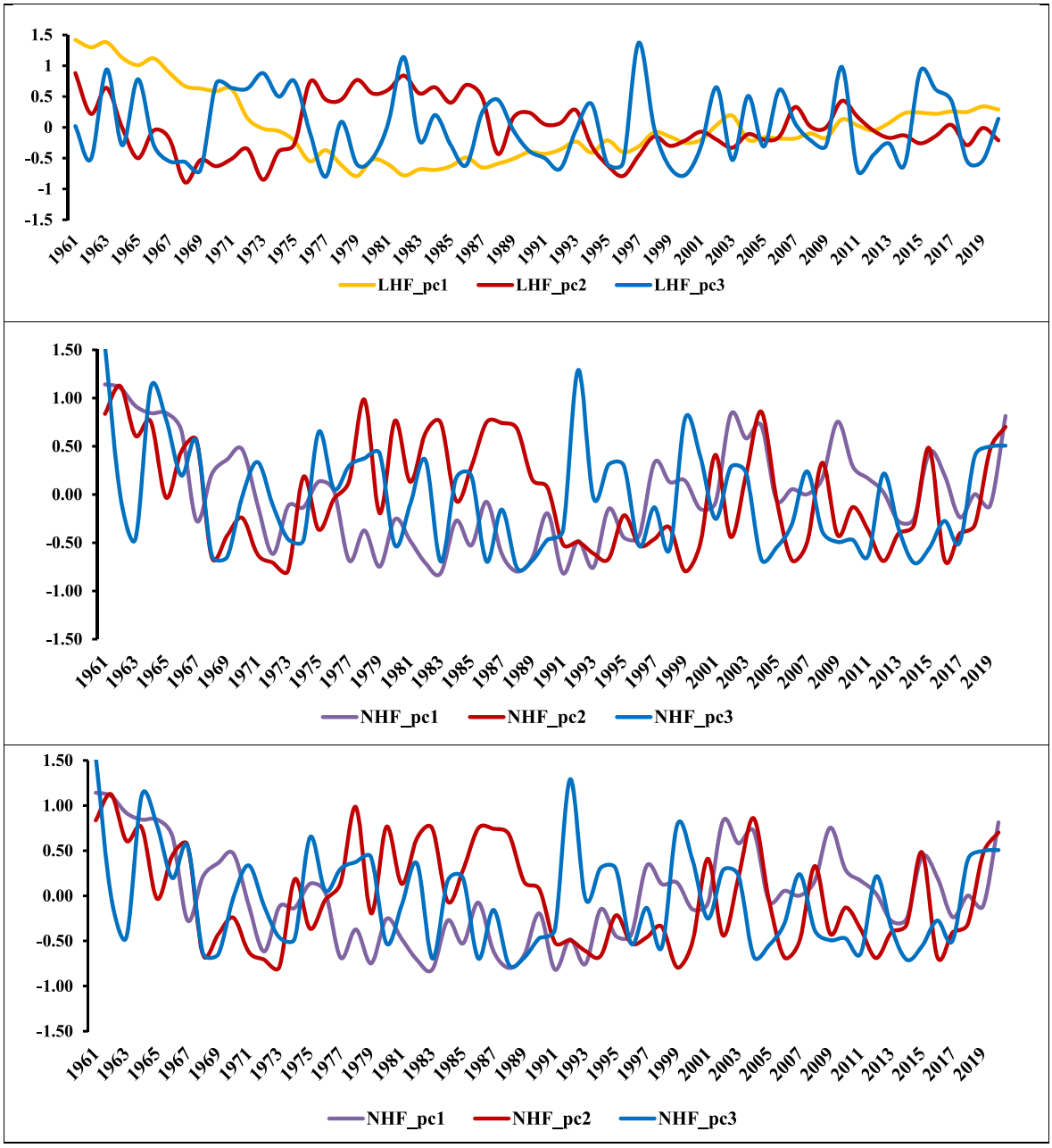

Fig. 9. (a) Normalized the first (yellow bar), the second (red bar) and the third (blue bar) principal components (PC)of NSW over the Indian region and its adjoining region during the summer monsoon season (period), (b) same as (a), but for the LHF, and (c) is same as (a), but for NHF.

informative since it effectively linked with vertical motion and subsequently gave rainfall. These findings provide process-level insights into the energy and moisture dynamics that govern the Indian Summer Monsoon system. The observed increases in MSE and moisture convergence over western and central India during the recent warming period are physically consistent with the enhanced LHF and positive NHF over nearby oceanic regions. These flux anomalies modulate near-surface pressure gradients, which in turn impact wind convergence and vertical motion, thereby facilitating deep convection. This chain of thermodynamic and dynamic adjustments is well-supported by monsoon energetics theory (e.g., Boos and Kuang, 2010; Trenberth et al., 2009), and reinforces the interpretation that the detected epochal variations are not random, but rather reflect evolving large-scale atmospheric processes. Thus, even in the absence of a modeling framework, these reanalysis-based diagnostics reveal meaningful physical linkages among surface fluxes, SST, low-level winds, and rainfall patterns under a changing climate.

4. Conclusions

This study unravels the tricadal and decadal evolution of large-scale monsoon circulation and energy balance over the Indian subcontinent and surrounding oceanic regions for the period 1961–2020. The results reveal that surface heat flux differences between land and ocean significantly shape the low-level monsoonal circulation in the tropics. Notably, these fluxes contribute to modulating the atmospheric heat source, pressure gradients, and moisture availability, all of which collectively influence convection and rainfall distribution during the Indian Summer Monsoon season. The spatial and temporal shifts in latent heat flux (LHF), sensible heat flux (SHF), net shortwave radiation (NSW), and net heat flux (NHF) show physically consistent associations with monsoon dynamics. For instance, increased LHF over the Arabian

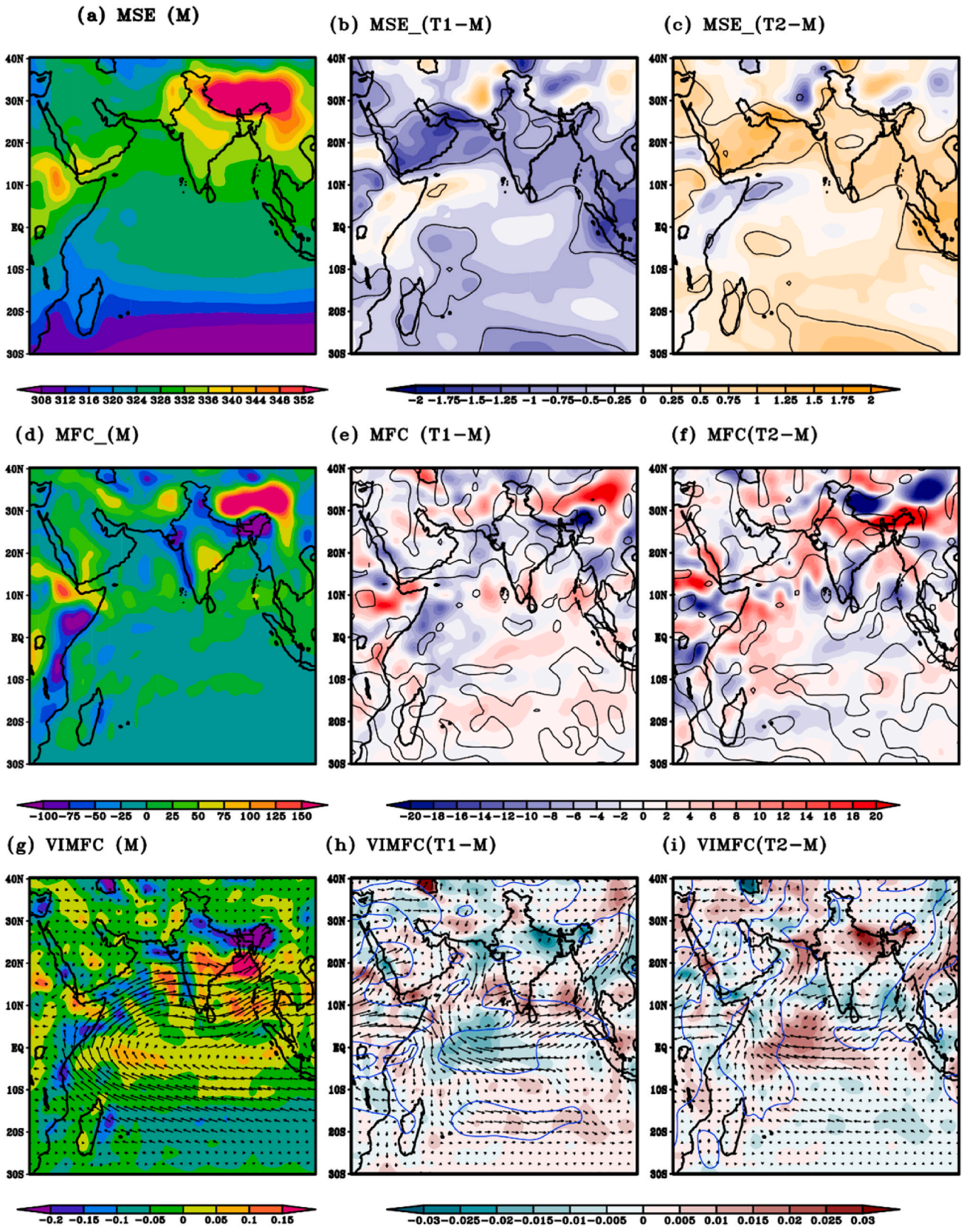

Fig. 10. (a–i): The climatological moist static energy (MSE, unit: KJKg-1) for (a) 1961–2020 (mean distribution (M)); (b) past tricade difference from mean (T1-M); (c) recent tricade difference from mean (T2-M), (Past tricade: T1; 1961–1990), (recent tricade: T2; 1991–2000); during JJAS. Moisture flux convergence (MFC; g/Kg-s) for (d) 1961–2020 (mean distribution (M)); (e) past tricade difference from mean (T1-M); (f) recent tricade difference from mean (T2-M). The climatological moisture flux (MF) (Kg/m2s; shaded) and vertically integrated moisture flux convergence (VIMFC) (Kg/m/s) for (g) 1961–2020 (mean distribution (M)); (h) past tricade difference from mean (T1-M); (i) recent tricade difference from mean (T2-M).The regions with 95 % confidence level are contoured.

Sea and eastern Indian Ocean in recent decades aligns with enhanced low-level moisture transport and convergent wind patterns over Western and Central India. This is further supported by higher Moist Static Energy (MSE) and positive rainfall anomalies in these regions, indicating more vigorous convective activity. Conversely, declining LHF and negative NHF over the Bay of Bengal correlate with reduced MSE and weakened monsoonal convection over northeastern India and the Gangetic plains. Quantitatively, the recent tricadal differences in surface heat fluxes are significant—for example, NSW increased by 10–12 W/m^2 over the Southern Peninsular India (SPI) and BoB, while decreasing by ~7 W/m^2 over the Southern Indian Ocean (SIO). NHF anomalies show positive trends over SPI (5 W/m^2) and BoB (20 W/m^2), and negative values over AS (−10 W/m^2) and EIO (−18 W/m^2). These anomalies correspond with rainfall increases of 0.7–1.0 mm/day over Western India, the Western Ghats, and parts of Central and Northeastern India. In contrast, rainfall decreased by −0.5 to −1.0 mm/day over NEI and SPI, consistent with reduced MSE and moisture flux convergence.

Additionally, the patterns of MFC and vertically integrated moisture flux (VIMFC) show that enhanced surface fluxes and oceanic warming have intensified the land-sea moisture gradient, leading to spatially heterogeneous rainfall trends. MSE and wind anomalies together confirm an increase in vertical moisture transport and convective potential, particularly over WI. These interlinked variations in SST, fluxes, wind fields, and moisture transport confirm that the observed epochal anomalies are not isolated trends but part of a dynamically coherent response of the monsoon system to long-term ocean–atmosphere coupling under climate change. While this study does not claim causality in a modeling framework, the diagnostics demonstrate process-consistent physical linkages between surface energy exchange and monsoon behaviour. These findings offer a valuable observational perspective on how warming-driven changes in land–ocean energetics and circulation dynamics may shape future ISMR variability. However, localized effects and internal variability introduce uncertainties that merit further exploration using high-resolution regional models and coupled ocean-atmosphere simulations. In addition to its scientific insights, this work supports the UN 2030 Agenda by contributing to SDG 13, SDG 2, and SDG 6. The analysis of monsoon-related surface flux variability offers valuable input for climate adaptation, food security, and water management strategies. This aligns with the growing body of scientific research supporting sustainability goals through climate diagnostics (Varotsos and Cracknell, 2020).

CRediT authorship contribution statement

R. Bhatla: Writing – review & editing, Visualization, Supervision, Resources, Methodology, Data curation, Conceptualization. **Archana Maurya:** Writing – original draft, Visualization, Software, Methodology, Investigation, Formal analysis, Data curation. **Aashna Verma:** Writing – review & editing, Formal analysis. **R.K. Mall:** Writing – review & editing, Visualization, Supervision, Resources, Methodology, Conceptualization. **Sanjay Bist:** Writing – original draft, Visualization, Resources, Investigation, Formal analysis, Data curation.

Declaration of competing interest

The authors declare that they have no known competing financial interests or personal relationships that could have appeared to influence the work reported in this paper.

Acknowledgments

The author expresses gratitude to the India Meteorology Department (IMD) for supplying essential gridded rainfall datasets and to ERA5 as well as NCEP/NCAR for providing the global reanalysis dataset. The authors also acknowledge IoE Grant (Scheme No. 6031), BHUfor providing funds.

Data availability

No data was used for the research described in the article.

References

Adames, Á.F., Ming, Y., 2018. Moisture and moist static energy budgets of South Asian monsoon low pressure systems in GFDL AM4. 0. J. Atmos. Sci. 75 (6), 2107–2123.
Albergel, C., Dutra, E., Munier, S., Calvet, J.C., Munoz-Sabater, J., de Rosnay, P., Balsamo, G., 2018. ERA-5 and ERA-interim driven ISBA land surface model simulations: which one performs better? Hydrol. Earth Syst. Sci. 22 (6), 3515–3532.
Annamalai, H., Slingo, J.M., Sperber, K.R., Hodges, K., 1999. The mean evolution and variability of the Asian summer monsoon: comparison of ECMWF and NCEP–NCAR reanalyses. Mon. Weather Rev. 127 (6), 1157–1186.
Banacos, P.C., Schultz, D.M., 2005. The use of moisture flux convergence in forecasting convective initiation: historical and operational perspectives. Weather Forecast. 20 (3), 351–366.
Barnett, T.P., 1978. Estimating variability of surface air temperature in the northern Hemisphere. Mon. Weather Rev. 106 (9), 1353–1367.
Bhatla, R., Mohanty, U.C., Raju, P.V.S., 2006. The variability of Indian Ocean surface meteorological fields during summer monsoon in EL Nino/La Nina years. Indian J. Mar. Sci. 35 (2), 93–103.
Bhatla, R., Raju, P.V.S., Mohanty, U.C., Madan, O.P., Mall, R.K., 2011. Study of energy fluxes over the Indian ocean prior and during the summer monsoon. Mar. Geod. 34 (2), 119–137.
Bhatla, R., Raju, P.V.S., Mall, R.K., Bist, S., 2016. Study of surface fluxes during onset of summer monsoon over India. Int. J. Climatol. 36 (4), 1821–1832.
Bhatla, R., Maurya, A., Sinha, P., Verma, S., Pant, M., 2022. Assessment of climate change of different meteorological state variables during Indian summer monsoon season. J. Earth Syst. Sci. 131 (2), 136.
Bollasina, M.A., Ming, Y., 2013. The role of land-surface processes in modulating the Indian monsoon annual cycle. Clim. Dyn. 41, 2497–2509.
Boos, W.R., Kuang, Z., 2010. Dominant control of the South Asian monsoon by orographic insulation versus plateau heating. Nature 463 (7278), 218–222.
Chakraborty, S., Saha, U., Maitra, A., 2015. Relationship of convective precipitation with atmospheric heat flux—a regression approach over an Indian tropical location. Atmos. Res. 161, 116–124.
Chang, C.P., 2011. The global monsoon system: research and forecast. World Scientific 5.
Chang, X., Wang, B., Yan, Y., Hao, Y., Zhang, M., 2019. Characterizing effects of monsoons and climate teleconnections on precipitation in China using wavelet coherence and global coherence. Clim. Dyn. 52, 5213–5228.
Dai, A., Fyfe, J.C., Xie, S.P., Dai, X., 2015. Decadal modulation of global surface temperature by internal climate variability. Nat. Clim. Change 5 (6), 555–559.
Deshpande, N.R., Kulkarni, J.R., 2022. Spatio-temporal variability in the stratiform/convective rainfall contribution to the summer monsoon rainfall in India. Int. J. Climatol. 42 (1), 481–492.
Fasullo, J., Webster, P.J., 2003. A hydrological definition of Indian monsoon onset and withdrawal. J. Clim. 16 (19), 3200–3211.
Folland, C.K., Karl, T.R., Christy, J.R., Clarke, R.A., Gruza, G.V., Jouzel, J., et al., 2001. Observed climate variability and change. Clim. Change 2001, 99.
Fontaine, B., Philippon, N., Camberlin, P., 1999. An improvement of June–September rainfall forecasting in the Sahel based upon region April–May moist static energy content (1968–1997). Geophys. Res. Lett. 26 (14), 2041–2044.
Gadgil, S., 2003. The Indian monsoon and its variability. Annu. Rev. Earth Planet Sci. 31 (1), 429–467.
Goswami, B.B., 2023. Role of the eastern equatorial Indian Ocean warming in the Indian summer monsoon rainfall trend. Clim. Dyn. 60 (1), 427–442.
Goswami, B.N., Chakravorty, S., 2017. Dynamics of the Indian summer monsoon climate. In: Oxford Research Encyclopedia of Climate Science.
Goswami, B.N., Kripalani, R.H., Borgaonkar, H.P., Preethi, B., 2016. Multi-decadal variability in Indian summer monsoon rainfall using proxy data. In: Climate Change: Multidecadal and Beyond, pp. 327–345.
Hersbach, H., Peubey, C., Simmons, A., Poli, P., Dee, D., Berrisford, P., 2018. ERA report series. https://www.ecmwf.int/en/forecasts/datasets/reanalysis-datasets/era-interim.
Hu, J., Duan, A., 2015. Relative contributions of the Tibetan Plateau thermal forcing and the Indian Ocean Sea surface temperature basin mode to the interannual variability of the East Asian summer monsoon. Clim. Dyn. 45, 2697–2711.
Huo, L., Guan, Z., Jin, D., Liu, X., Wang, X., Xia, Y., 2022. The interdecadal variations and causes of the relationship between autumn precipitation anomalies in eastern China and SSTA over the southeastern tropical Indian Ocean. Clim. Dyn. 1–13.
Intergovernmental Panel on Climate Change (IPCC), 2013. Climate Change 2013: the Physical Science Basis. Contribution of Working Group I to the Fifth Assessment Report of the Intergovernmental Panel on Climate Change. Cambridge Univ. Press, Cambridge, U. K., and New York, p. 1535.
Jalihal, C., Srinivasan, J., Chakraborty, A., 2019. Modulation of Indian monsoon by water vapor and cloud feedback over the past 22,000 years. Nat. Commun. 10 (1), 5701.
Johari Chan, K., 2020. The intraseasonal variability of the Indian summer monsoon: dynamics, thermodynamics and land-atmosphere-ocean interactions. (Doctoral dissertation, University of Reading).
Joseph, P.V., 2014. Role of ocean in the variability of Indian summer monsoon rainfall. The earth's hydrological cycle 723–738.

Kalnay, E., Kanamitsu, M., Kistler, R., Collins, W., Deaven, D., Gandin, L., et al., 1996. The NCEP/NCAR 40-year reanalysis project. Bull. Am. Meteorol. Soc. 77 (3), 437–472.
Karmakar, N., Misra, V., 2020. Differences in northward propagation of convection over the Arabian Sea and Bay of Bengal during boreal summer. J. Geophys. Res. Atmos. 125 (3), e2019JD031648.
Krishnamurthy, L., Krishnamurthy, V.J.C.D., 2014. Influence of PDO on South Asian summer monsoon and monsoon–ENSO relation. Clim. Dyn. 42, 2397–2410.
Krishnamurti, T.N., Sikka, D.R., 1978. Some Aspects of the Life History, Structure and Movement of Monsoon Depressions. Monsoon dynamics, pp. 1501–1529.
Leetmaa, A., Reynolds, R., Jenne, R., Josepht, D., 1996. The NCEP/NCAR 40-year reanalysis project. Bull. Am. Meteorol. Soc. 77, 437–471.
Liu, J., Curry, J.A., 2006. Variability of the tropical and subtropical ocean surface latent heat flux during 1989–2000. Geophys. Res. Lett. 33 (5).
Malik, A., Brönnimann, S., Stickler, A., Raible, C.C., Muthers, S., Anet, J., et al., 2017. Decadal to multi-decadal scale variability of Indian summer monsoon rainfall in the coupled ocean-atmosphere-chemistry climate model SOCOL-MPIOM. Clim. Dyn. 49, 3551–3572.
Maurya, A., Verma, S., Pant, M., Bhatla, R., 2023. Epochal changes in the intrinsic nature/dynamics of flood and drought during Indian summer monsoon. Earth Space Sci., e2022EA002674
Meehl, G.A., Hu, A., 2006. Megadroughts in the Indian monsoon region and southwest North America and a mechanism for associated multidecadal Pacific sea surface temperature anomalies. J. Clim. 19 (9), 1605–1623.
Mohanty, U.C., Ramesh, K.J., Kumar, N.M., Potty, K.V.J., 1994. Variability of the Indian summer monsoon in relation to Oceanic heat budget over the Indian seas. Dynam. Atmos. Oceans 21 (1), 1–22.
Mohanty, U.C., Ramesh, K.J., Pant, M.C., 1996. Certain seasonal characteristic features of Oceanic heat budget components over the Indian seas in relation to the summer monsoon activity over India. Int. J. Climatol. 16 (3), 243–264.
Mohanty, U.C., Nayak, H.P., Sinha, P., Osuri, K.K., Niyogi, D., 2019. Land surface processes over Indian summer monsoon region: a review. Mausam 70 (4), 691–708.
Pai, D.S., Rajeevan, M., Sreejith, O.P., Mukhopadhyay, B., Satbha, N.S., 2014. Development of a new high spatial resolution (0.25× 0.25) long period (1901-2010) daily gridded rainfall data set over India and its comparison with existing data sets over the region. Mausam 65 (1), 1–18.
Pant, M., Bhatla, R., Ghosh, S., Das, S., Mall, R.K., 2023. Will warming climate affect the characteristics of summer monsoon rainfall and associated extremes over the Gangetic Plains in India? Earth Space Sci. 10 (2), e2022EA002741.
Rao, K.G., Reddy, N.N., 2019. On moisture flux of the Indian summer monsoon: a new perspective. Geophys. Res. Lett. 46 (3), 1794–1804.
Roxy, M.K., Ritika, K., Terray, P., Murtugudde, R., Ashok, K., Goswami, B.N., 2015. Drying of Indian subcontinent by rapid Indian Ocean warming and a weakening land-sea thermal gradient. Nat. Commun. 6 (1), 7423.
Roy, I., Tedeschi, R.G., Collins, M., 2019. ENSO teleconnections to the Indian summer monsoon under changing climate. Int. J. Climatol. 39 (6), 3031–3042.
Sharmila, S., Joseph, S., Sahai, A.K., Abhilash, S., Chattopadhyay, R., 2015. Future projection of Indian summer monsoon variability under climate change scenario: an assessment from CMIP5 climate models. Global Planet. Change 124, 62–78.
Singh, C.V., 2004. Empirical Orthogonal Function (EOF) analysis of monsoon rainfall and satellite-observed outgoing long-wave radiation for Indian monsoon: a comparative study. Meteorol. Atmos. Phys. 85 (4), 227–234.
Sobel, A.H., Nilsson, J., Polvani, L.M., 2001. The weak temperature gradient approximation and balanced tropical moisture waves. J. Atmos. Sci. 58 (23), 3650–3665.
Sooraj, K.P., Seo, K.H., 2013. Boreal summer intraseasonal variability simulated in the NCEP climate forecast system: insights from moist static energy budget and sensitivity to convective moistening. Clim. Dyn. 41, 1569–1594.
Trenberth, K.E., Guillemot, C.J., 1998. Evaluation of the atmospheric moisture and hydrological cycle in the NCEP/NCAR reanalyses. Clim. Dyn. 14, 213–231.
Trenberth, K.E., Dai, A., Rasmussen, R.M., Parsons, D.B., 2003. The changing character of precipitation. Bull. Am. Meteorol. Soc. 84 (9), 1205–1218.
Trenberth, K.E., Fasullo, J.T., Kiehl, J., 2009. Earth's global energy budget. Bull. Am. Meteorol. Soc. 90 (3), 311–324.
Turner, A.G., Annamalai, H., 2012. Climate change and the South Asian summer monsoon. Nat. Clim. Change 2 (8), 587–595.
Varotsos, C.A., Cracknell, A.P., 2020. Remote sensing letters contribution to the success of the sustainable development Goals-UN 2030 agenda. Remote Sensing Letters 11 (8), 715–719.
Verma, A., Vishwakarma, A., Bist, S., Kumar, S., Bhatla, R., 2023. A long-term drought assessment over India using CMIP6 framework: present and future perspectives. Mausam 74 (4), 963–972.
Wang, T.M., Wu, G.X., 2008. Land-sea thermal contrast over South Asia and its influences on tropical monsoon circulation. J. Trop. Meteorol. 24, 37–43.
Weare, B.C., Strub, P.T., Samuel, M.D., 1981. Annual mean surface heat fluxes in the tropical Pacific Ocean. J. Phys. Oceanogr. 11 (5).
Webster, P.J., 1994. The role of hydrological processes in ocean-atmosphere interactions. Rev. Geophys. 32 (4), 427–476.
Wu, R., Jiao, Y., Wang, Y., Jia, X., 2020. High-frequency wind-related seasonal mean latent heat flux changes over the tropical Indo-western Pacific in El Niño and La Niña years. J. Geophys. Res. Atmos. 125 (21), e2020JD032954.
Yanai, M., Tomita, T., 1998. Seasonal and interannual variability of atmospheric heat sources and moisture sinks as determined from NCEP–NCAR reanalysis. J. Clim. 11 (3), 463–482.
Yang, S., Wu, R., Jian, M., Huang, J., Hu, X., Wang, Z., Jiang, X., 2020. Climate Change in Southeast Asia and Surrounding Areas. Springer Nature.
Zeng, J., Zhang, Q., 2020. The trends in land surface heat fluxes over global monsoon domains and their responses to monsoon and precipitation. Sci. Rep. 10 (1), 5762.